

Application of Similitude Laws for The Design of Electromechanical Models Using High-Temperature Superconductors

Pedro Rocha
pedro.rocha@ist.utl.pt

Instituto Superior Técnico, Lisboa, Portugal

January 2021

Abstract

The use of superconducting materials for implementation on electric machines is nowadays a relevant subject of research, for the design of new, more efficient, and power dense machines. Based on the physical behaviours of superconductors being more complex than conventional magnetic materials present in electric machines, preliminary and qualitative studies are necessary to compare the new potential superconducting electrical machines to conventional ones.

The aim of this paper is, then, to make a comparative study of both types of machines, using similitude laws, also called scale laws. This dissertation presents the study of similitude laws for high temperature superconductors (HTS) inserted in electric machines. First, scale laws are presented for the case of electric machines with permanent magnets. Then, HTS are introduced, as well as the scale laws representative of their losses regarding current density, magnetic flux density and volume. This study was made using a simplified analytical model, the Kim model. Second, the comparison between conventional machines and machines using HTS, being as permanent magnets, or as coils was performed. Third, experimental tests were performed, to quantify and validate the losses in YBCO bulks, also with additional validation on FEM simulations.

It was found by scale laws that HTS electric machines are indicative of having higher efficiencies and more power dense, however, the machine's topologies need to be different, especially using HTS as permanent magnets. The experimentations were inconclusive, as well as the FEM simulations, which indicates that a more precise and complex experiments need to be performed.

Keywords: Similitude Laws, High Temperature Superconductors (HTS), YBCO, Hysteresis Losses

1. Introduction

1.1. Motivation

Superconducting electromechanical machines have been researched since the 1950s for applications where higher efficiency and power density is required, however only with the discovery of the high temperature superconductors (HTS) in 1986, there was a major development in electric power applications. At this time were created the first HTS synchronous machines where an HTS field excitation winding can provide high magnetic flux density in the air gap with major reductions of excitation losses, this type of performance was unachievable with traditional field excitation systems, like copper coils or permanent magnets (PM). A PM motor rated at 7 MW for marine pod propulsor weighs about 120 tonnes, when an HTS synchronous motor concept would drastically reduce

the weight of a podded electromechanical drive by 50% [4]. Another approach is the design of a synchronous reluctance machine with HTS bulk in the rotor. In synchronous reluctance machines, the rotor moves towards a position favouring a value of maximum magnetic flux. The torque produced by these machines is proportional to the difference between the stator inductance maximum value, L_{max} , and the minimum value L_{min} . It is possible to amplify this difference by using bulk HTS blocks on the rotor. The diamagnetic properties of superconductors make them ideal, leading to an increase of the L_{max} , which results in an increase of torque. In the last years had been a development in HTS machine solutions for industrial applications, the first HTS industrial motor rated at 1.2 MW was built by Rockwell Automation, and for energy production, like the 4MVA HTS generator developed by

Siemens [9][1]. Another relevant subject is similitude (or scaling) laws. They are used to predict the performance of a new design based on data from an existing, similar design. In the electromagnetics, new design and similar design will have a similar geometry, but in general not the same materials and electromagnetic excitation [6]. This subject is very used in synchronous permanent magnet machines built to offshore wind turbines to maximize the relation available power and occupied volume (or weight) and for reducing the operational costs [3]. It is also used in switched reluctance motors (SRM) [5].

2. Similitude Laws

The focus of this subsection will be to understand how the machine efficiency can be maximized with the increase of size and with the use of a modular configuration in a machine with PM.

2.1. Singular Configuration

The nominal power in a generic PM machine is given through the relation (1)

$$P_N \propto l^4 \quad (1)$$

where the number of phases, number of pole pairs, the electric frequency, the magnetic flux density and the current density are kept constant and l is the characteristic length.

The joule losses in PM machines are due to the current that flows through the copper conductors and the relation is given by (2)

$$P_J \propto l^3 \quad (2)$$

Considering the efficiency due to joule losses as

$$\eta_J = \frac{1}{1 + \frac{P_J}{P_N}} \quad (3)$$

the final efficiency considering the characteristic length is given through (4)

$$\eta_J = \frac{1}{1 + \frac{K_1}{l}} \quad (4)$$

where $K_1 = 0.099$ in order to have a normalized efficiency, at $l = 1$, of 91%.

The total efficiency considers the iron losses, which have the same behaviour in function of characteristic length as joule losses, are given by (5)

$$\eta_T = \frac{1}{1 + \frac{3K_1}{l}} \quad (5)$$

2.2. Modular Configuration

Another approach for a drive system is to have a modular configuration, i.e., multiple machines mechanically connected to achieve the same mechanical power and torque.

The modular power, P_m , which represents the power of each module, is given by (6)

$$P_m = \frac{P}{n} \quad (6)$$

and the ratio between volumes is given by (7)

$$\frac{V_m}{V} = \left(\frac{l_m}{l}\right)^3 = \frac{1}{(\sqrt[4]{n})^3} \quad (7)$$

where V_m is the volume of a module and V is the volume of a single machine configuration.

Figure 1 shows the comparison between power ratio and volume ratio.

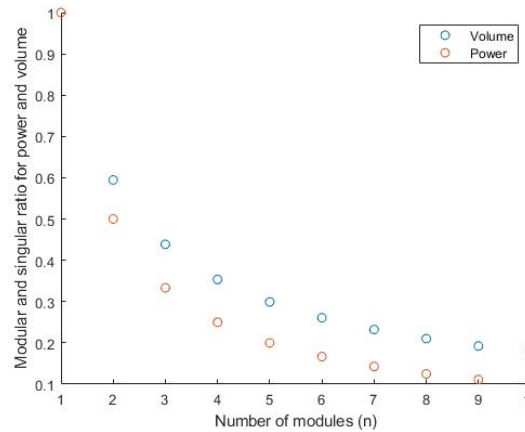


Figure 1: Modular and singular ratio for power and volume

It is possible to conclude that with the increase of modules, it is necessary a increase of volume to reach the same power.

Considering the joule losses in the modular configuration it is possible to define the efficiency in function of modules, as equation (8) shows.

$$\eta_{mT} = \frac{1}{1 + \frac{n^{0.25} P_J}{P_N}} \quad (8)$$

Figure 2 shows the relationship between the total modular efficiency with respect to the number of models. In this figure, the efficiency of the single machine is considered to be $\eta = 91\%$.

It is possible to conclude that the module configuration shows a decreasing in efficiency with the increasing of number of modules.

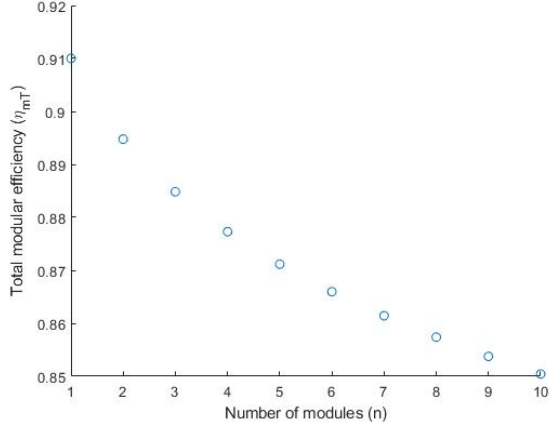


Figure 2: Relation between total module efficiency η_{mT} and the number of modules n

3. High Temperature Superconductors

3.1. E-J Power Law for HTS

In HTS, the relation between \mathbf{E} and \mathbf{J} is non-linear and is defined by

$$E = E_0 \left(\frac{J}{J_C} \right)^m \quad (9)$$

where E_0 is the electric field that defines the critical current density, m is the power constant and J_C is the critical current density, which depends on the magnetic field density inside the superconductor, as well as its temperature [10].

The critical current density is a function of temperature, T , and the magnetic flux density, B , as shown in (10)

$$J_C(B, T) = J_{C0\beta} \left(1 - \left(\frac{T}{T_C} \right)^2 \right)^{\frac{3}{2}} \left[\frac{B_0}{B_0 + B} \right] \quad (10)$$

where $J_{C0\beta}$ represents the critical current density at 0 K with no applied field and B_0 the value of the applied magnetic flux density that reduces the value of the critical current density to half of its maximum value [1].

3.2. KIM Electromagnetic Model

Considering an external magnetic field, H_a , defined as (11)

$$H_a = H_m \sin(\omega t) \quad (11)$$

where H_m is the amplitude of the waveform, ω the angular frequency and t time.

This external magnetic field is applied to an HTS bulk along the z axis, like shown in figure 3.

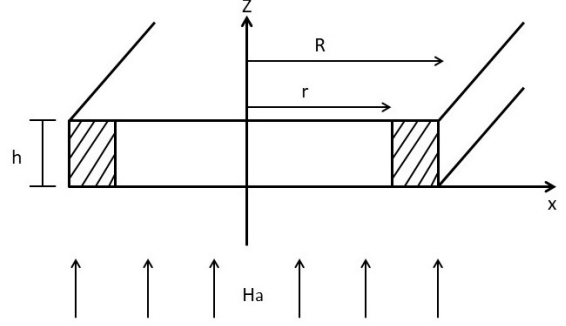


Figure 3: Superconductor bulk representation

In this configuration, the magnetic quantities have only z components, and the induced currents have only x and y components. This model involves only macroscopic induced currents, magnetization, flux density, and field.

The applied magnetic field, H_a , is defined as

$$H_a = \frac{B}{\mu_0} \quad (12)$$

where B is the macroscopic flux density and μ_0 is permeability of free space. If H_a is the applied magnetic field and M_i is the local magnetization, that is, the field produced by bulk induced currents, the equation (13) relates these variables with H , the local magnetic field inside the bulk [?]

$$H = \frac{B}{\mu_0} + M_i \quad (13)$$

The total magnetization M is the average of M_i over the sample cross section.

The induced currents density J , the H and the M_i along a given circuit are uniform and are written as functions of x : $J(x)$, $H_i(x)$, and $M_i(x)$.

The magnetization $M_i(x)$ can be found through (14)

$$M_i(x) = \int_r^R J_i(x) dx \quad (14)$$

The $J(x)$ is given through (15)

$$J(x) = \frac{\text{sgn}(J)k_1}{\sqrt{(H_0)^2 - \text{sgn}(JH_i)2k_1(x+c)}} \quad (15)$$

where c is an integration constant to be determined by the boundary conditions and where k_1 and H_0 are constants.

Considering the initial state, where $H_a=M=0$ and increase H_a in z direction. According to Faraday's Law, the induced currents J , with negative sign, will penetrating the bulk from the surface inward. Considering now that these induced currents

only penetrates until a certain $x = r$, this means that the local internal field, H_i , in the bulk will be H_m at $x = R$, decreasing to 0 until $x = r$ and remains in that value for $x < r$. If the value of H_m increases, r will be decrease. This means that when $r = 0$, the bulk is completely full-penetrated and H_p is the corresponding field [2].

The value of H_p is defined as

$$H_p = \sqrt{(H_0)^2 + 2k_1 r} - H_0 \quad (16)$$

where r is the radius of the cylindrical YBCO and k_1 is a variable that depends on the temperature.

Through the software MATLAB, it was developed a code, that can generate the M-H curve for different radius dimension and for different external magnetic fields. Additionally, the code presents in real time the variation of $J_i(x)$ and $B_i(x)$ in function of the radius as shown in figure 4.

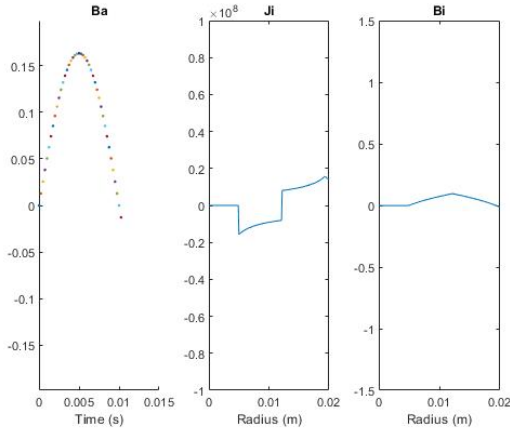


Figure 4: Figure from Matlab code for M-H analytic curve.

In figure 5 is represented an example of the M-H curves generated through the KIM model.

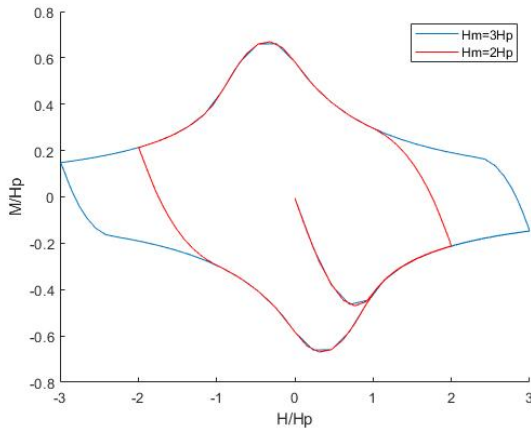


Figure 5: M-H curves examples

3.3. Hysteresis Losses

In the electromagnetic model considered, the hysteresis losses will be associated with H_i and its variation when subject to a time-variant external applied magnetic field, H_a . To compute the hysteresis loops for different values of H_m , it will be used the equations for $J_i(x)$ and $H_i(x)$ defined in [2].

The figure 6 is a YBCO generic M-H for $H_m \leq H_p$.

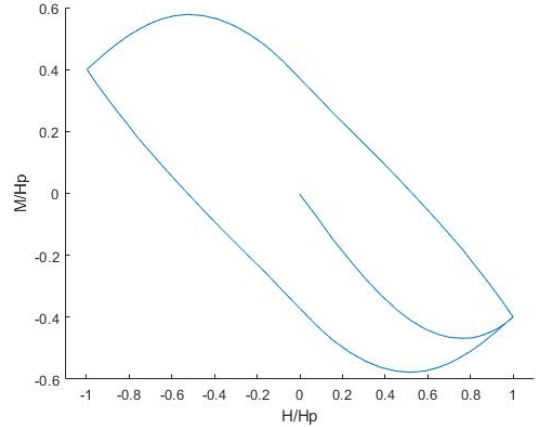


Figure 6: Generic M-H curve for YBCO, scaled by H_p , for $H_m \leq H_p$.

It is possible to see through figure 6 that the magnetization response to the applied magnetic field is different in YBCO and in a ferromagnetic material. In YBCO, when H_a increases, the magnetization decreases for negative values to cancel the imposed magnetic field inside the bulk. When H_a decreases, the magnetization increases until H_a increases again.

The total hysteresis losses will be calculated through the integration of the area inside the loop, as given in equation (17) [1]

$$W_H = \oint B dM = \oint \mu_0 H dM \quad [J/m^3/cycle] \quad (17)$$

The use of different frequencies is common, in this cases is necessary to see the result of 17 as a power density loss

$$P_H = f \oint B dM \quad [W/m^3] \quad (18)$$

3.4. Implementation Examples

In figure 7 is represented the M-H curves for different radius, r , for $H_m = H_p$.

Considering that the temperature remains the same, the increase of the radius dimensions leads to an increase in the value of H_p , this means that is possible to achieve higher magnetization than in

smaller radius without changing the shape of the curve M-H.

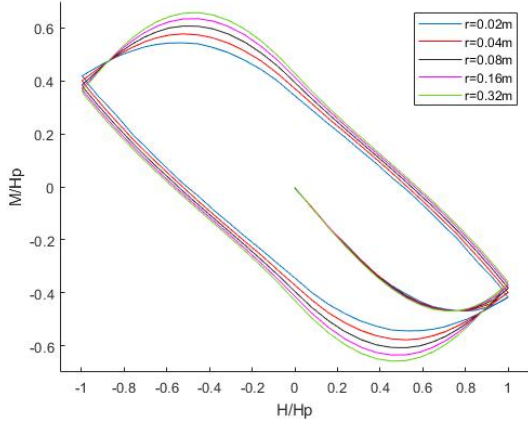


Figure 7: M(H) curves for different radius and for $H_m=H_p$

The figure 8 shows the curve M(B) for different applied magnetic flux densities keeping the radius constant.

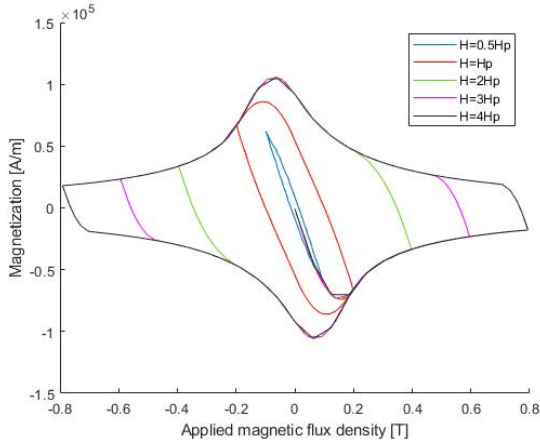


Figure 8: M(B) curve for different ratio of penetration with $r=0.02m$

The next step is study the relation of hysteresis losses with the increasing of radius and magnetic penetration ($\frac{H}{H_p}$). Figure 9 represent this relation.

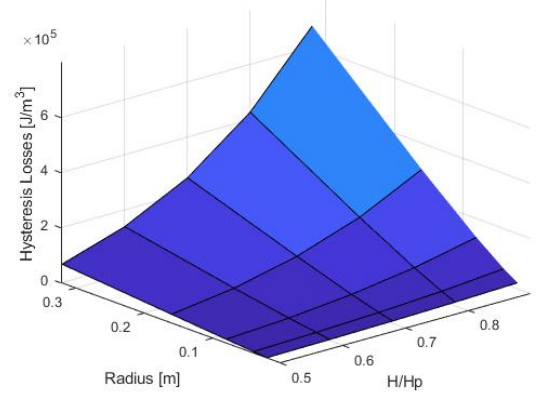


Figure 9: 3D plot for radius, ratio of penetration and hysteresis losses

As expected, the higher value for hysteresis losses occurs for the maximum ratio of magnetic penetration and for the maximum radius' size.

4. Similitude Laws for YBCO

4.1. Magnetic Density Flux Constant

Figure 10 shows several acquired data from the MATLAB code for hysteresis losses in function of volume, always keeping the average value of magnetic density flux in YBCO bulk constant, and the correspondent fitting curve.

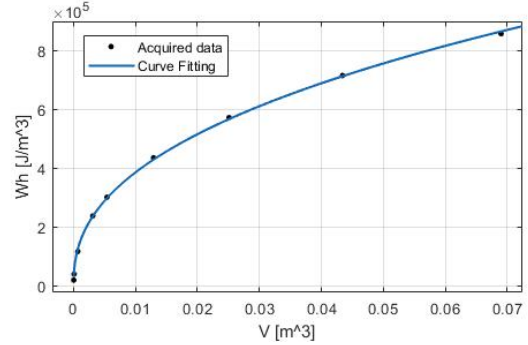


Figure 10: Acquired data for hysteresis losses in function of volume and the best curve fitting

The equation that fits better the above points is give by,

$$W_h = 2.6 \times 10^5 \times V^{0,4175} \quad (19)$$

thus the variation of hysteresis losses with the volume is given by (20)

$$W_H \propto V^{0,4175} \quad (20)$$

Considering the same conditions for P_N as in chapter 2

$$\frac{P_H}{P_N} \propto \frac{l^{1,253}}{l^4} \propto l^{-2,75} \quad (21)$$

The relation for the efficiency of YBCO in function of linear dimension is given by (31).

$$\eta_{YBCO} = \frac{1}{1 + \frac{K_1}{l^{2,75}}} \quad (22)$$

Figure 11 shows a comparison between the efficiency of a machine if only hysteresis losses in YBCO or only joule losses in the conductors are considered.

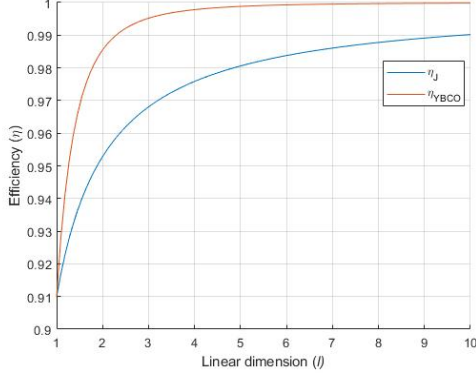


Figure 11: Efficiency comparison between YBCO and joule losses in conductors.

If it is considered a modular configuration the respective efficiency is give by relation (23).

$$\eta_{mT} \cong \frac{1}{1 + \frac{n^{0,687} P_H}{P_N}} \quad (23)$$

In figure 12 is represented the comparison between the joule losses with temperature constraints and the hysteresis losses for YBCO in function of the number of modules when considered a singular configuration efficiency with $\eta = 91\%$.

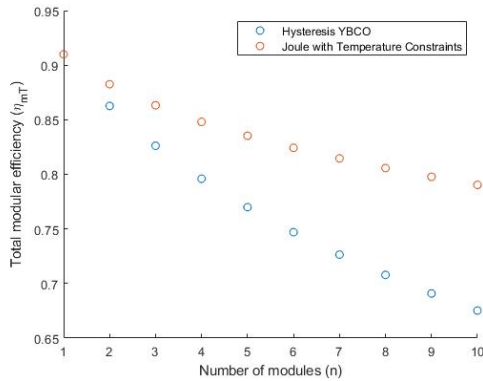


Figure 12: Comparison between the joule losses with temperature constraints and the hysteresis losses for YBCO in function of the number of modules

It is possible to conclude that the modular configuration for YBCO leads to a decreasing efficiency

when compared with joule losses. This substantial decrease occurs because when the number of modules increases, there is a reduction in the linear dimension, for each module, but the magnetic flux density is constant in all, this leads to an increase in losses that leads to a decrease in efficiency.

If a machine with YBCO instead of PM is considered, the equation 24 defines the total losses.

$$P_T = P_{iron} + P_{Jcoil} + P_{HYBCO} \quad (24)$$

The relation for the efficiency of a machine with YBCO in function of linear dimension is given by (25).

$$\eta_\alpha = \frac{1}{1 + K_1 \left(\frac{3}{l} + \frac{1}{l^{2,75}} \right)} \quad (25)$$

In figure 13 is represented the comparison between the efficiency of a machine with PM and a machine with YBCO instead of PM.

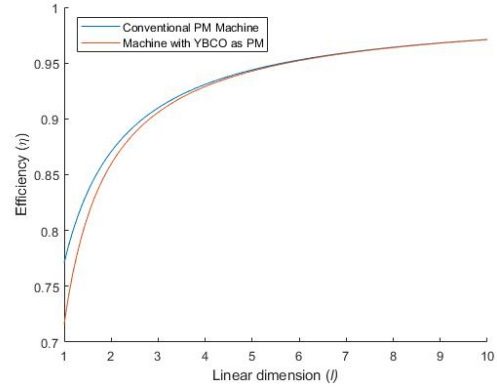


Figure 13: Efficiency for machine with PM and with YBCO

4.2. Current Density Constant

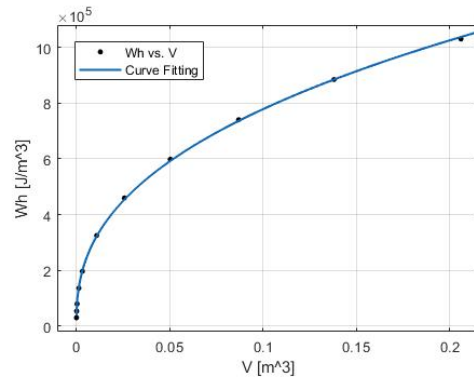


Figure 14: Acquired data for hysteresis losses in function of volume and the best curve fitting for the situation with current density constant

The final expression that relates the hysteresis losses with dimension is given through (26)

$$P_{HJ} \propto l^{1.17} \quad (26)$$

Considering the same conditions for P_N as in chapter 2

$$\frac{P_{HJ}}{P_N} \propto l^{-2.83} \quad (27)$$

The relation for the efficiency of YBCO, considering current density constant inside, in function of linear dimension is given by (28).

$$\eta_{YBCOJ} = \frac{1}{1 + \frac{K_1}{l^{2.83}}} \quad (28)$$

Figure 15 shows a comparison between the efficiency of a machine if only hysteresis losses in YBCO or only joule losses in the conductors are considered, for density current constant.

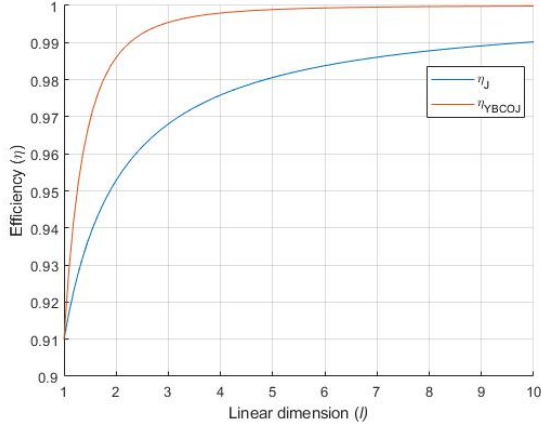


Figure 15: Efficiency comparison between YBCO and joule losses in conductors for density current constant

The respective efficiency of this modular configuration is give by relation (29).

$$\eta_{mT} \cong \frac{1}{1 + \frac{n^{0.708} P_H}{P_N}} \quad (29)$$

In figure 16 is represented the comparison between total modular efficiency of a machine where YBCO replaces the PM and a machine where YBCO replaces the coils. It was considered a singular configuration efficiency with $\eta = 91\%$.

It is possible to conclude that with the increase of modules, the efficiency of a machine with YBCO as coils starts to decreases when compared with another with YBCO as PM.

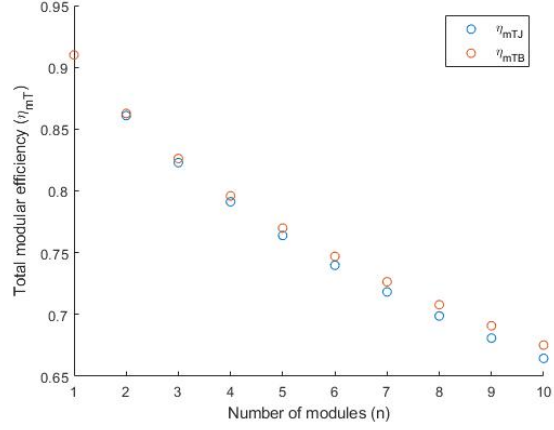


Figure 16: Modular efficiency in function of number of modules

If a machine with YBCO instead of copper coils is considered, the equation (30) defines the total losses.

$$P_T = P_{iron} + P_{HYBCO} \quad (30)$$

The relation for the efficiency of a machine with YBCO as coils in function of linear dimension is given by (31)

$$\eta_\beta = \frac{1}{1 + K_1 \left(\frac{2}{l} + \frac{1}{l^{2.83}} \right)} \quad (31)$$

In figure 17 is represented the comparison between the efficiency of a conventional PM machine, a machine with YBCO as PM and a machine with YBCO as coils.

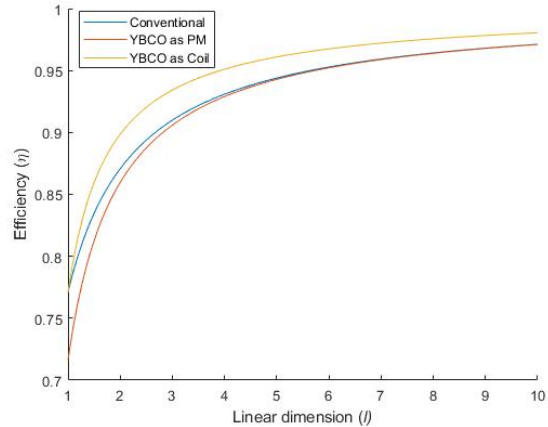


Figure 17: Efficiency of a conventional PM machine, a machine with YBCO as PM and a machine with YBCO as coils with increase of linear dimension.

It is possible to conclude that for smaller linear dimension values there is a difference, especially for YBCO as a coil. This happens because the in

this machine there aren't copper losses, enabling a higher value of efficiency. However, with the increase of linear dimension, the iron losses start to be the dominant factor, leads to a convergence in efficiency with the other machine designs.

5. Experimental and FEM simulations

5.1. Iron Core Experimental

In this subsection, it will be present a solution for estimation of YBCO losses through the utilization of an iron core magnetic circuit.

The idea was using two different magnetic circuits, one with an air-gap and the other with the YBCO in the space of the air-gap, as present in figures 18 and 19, and compared the losses in both circuits.



Figure 18: Experimental magnetic iron core circuit

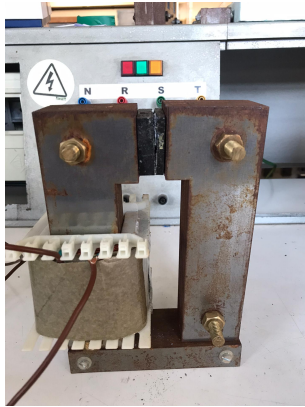


Figure 19: Experimental magnetic iron core circuit with YBCO

The total power in the magnetic circuit of the figure 18 is

$$P_T = P_{Cu} + P_{iron} \quad (32)$$

where P_{Cu} are the joule losses in the copper windings and P_{iron} are the iron losses, that are mostly composed by hysteresis losses due to the fact that the core is laminate.

The total power in the magnetic circuit of the figure 19 is

$$P_T = P_{Cu} + P_{iron} + P_{YBCO} \quad (33)$$

In the table 1 are presented the power and respective losses at ambient temperature for the configuration illustrated in figure 18. To measured these values was used a Fluke 1735 Three-Phase Power Quality Logger.

Table 1: Power and losses at air temperature for circuit iron + coil with air-gap

P_T [W]	P_{Cu} [W]	P_{iron} [W]
9	5.19	3.81
35	20.2	14.8
75	42.77	32.23
125	68.95	56.05

With table 1 is possible to compute the power factor of the circuit and this value will be considered the same for the cooled magnetic circuit with YBCO and without. The coil resistance was measured in temperature ambient and cooled, having 1.5Ω and 0.3Ω , respectively.

The first measurement in a cooled environment was without YBCO and the results are shown in table 2.

Table 2: Power and losses for cooled circuit iron + coil with air-gap

P_T [W]	P_{Cu} [W]	P_{iron} [W]
167.65	20.92	146.73

In the second measurement was introduced the YBCO in the air-gap position, as illustrated in figure 19. It was considered that the iron losses remain the same. With these conditions, it was possible to compute the losses regarding to YBCO, as shown in table 3

Table 3: Power and losses for cooled circuit iron + coil+ YBCO

P_T [W]	P_{Cu} [W]	P_{iron} [W]	P_{YBCO} [W]
173.28	22.34	146.73	4.21

Considering that YBCO bulk as a volume of $13.5cm^3$, the power density losses in YBCO are $3.1 \times 10^5 W/m^3$.

When compared with the analytic value for the same applied magnetic field, there is a considerable difference since the analytic value is $4.3 \times 10^4 W/m^3$. This can happen due to multiple factors, one of

them can be associated with the lack of accuracy in the measurement due to the chosen set up or the measurement instruments, the second factor can be related with some considerations made to compute the YBCO losses, like iron losses or power factor constant values, and the last factor can be related with the value founded through the analytic model since this model isn't extremely accurate for low magnetic field values.

5.2. FEM simulations

The Jiles-Atherton model [8] is a model that defines the curve B-H of a material with hysteresis through an analytic model, this will be the model used to define the B-H curve for the iron core. For that, the model finds the magnetization derivative in function of the applied magnetic field, known as susceptibility, χ , through the following equations,

$$H_e = H + \alpha M \quad (34)$$

$$M_{an} = M_s \left(\coth \frac{H_e}{a} - \frac{a}{H_e} \right) \quad (35)$$

$$\frac{dM_{an}}{dH_e} = \frac{M_s}{a} \left[1 - \left(\coth \frac{H_e}{a} \right)^2 + \left(\frac{a}{H_e} \right)^2 \right] \quad (36)$$

$$\frac{dM_{irr}}{dH} = \frac{M_{an} - M}{k\delta(1-c) - \alpha(M_{an} - M)} \quad (37)$$

$$\chi = \frac{dM}{dH} = \left[c \frac{dM_{an}}{dH_e} + (1-c) \frac{dM_{irr}}{dH} \right] \frac{1}{1-ac} \quad (38)$$

where H is the applied magnetic field, M is the magnetization, M_s is the magnetization saturation, M_{an} is the anhysteretic magnetization, M_{irr} is the irreversible magnetization, δ is a parameter that depend on the signal of $\frac{dH}{dt}$ and α, a, c and k are the unknown parameters that change the shape of the B-H curve, for different materials. To find this parameters that generates the B-H curve that better fits the experimental one, the algorithm in [7] and the Matlab/Simulink non-linear inductor were used.

In table 4 are shown the Jiles-Atherton parameters that better fit the experimental iron core.

Table 4: Jiles-Atherton iron parameters

Parameters	
M_s	$1.1827 \cdot 10^6$ [A/m]
a	61.86 [A/m]
k	900 [A/m]
c	0.04
α	$2 \cdot 10^{-4}$

The 3D model used will be the one represented in figure 20 surrounding by air. It will be a time dependent simulation, where the magnetic field is generated through the coil. The B-H curve for the iron core is defined through the Jiles-Atherton model using the parameters in table 4.

A voltage of 300V at 50Hz was applied in the coil and it was considered a 0.02s simulation to eliminate all the transient components.

In figures 20 is represented simulation results considering the magnetic flux density.

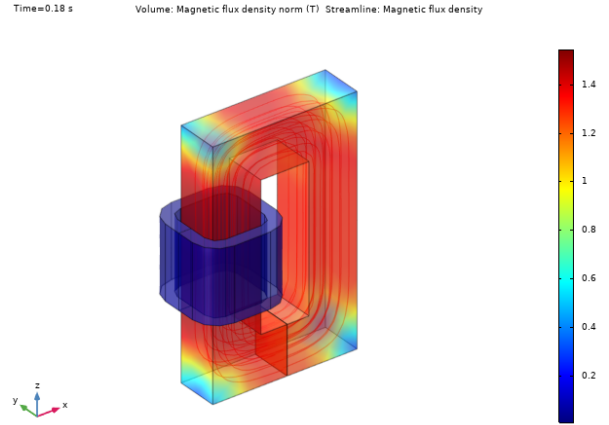


Figure 20: Magnetic flux density norm and streamlines results for an isometric view

In figure 21 are represented two B-H curves, at blue the experimental one and at red the one generates through the FEM software simulation. These two curves have a difference in hysteresis losses of 12%.

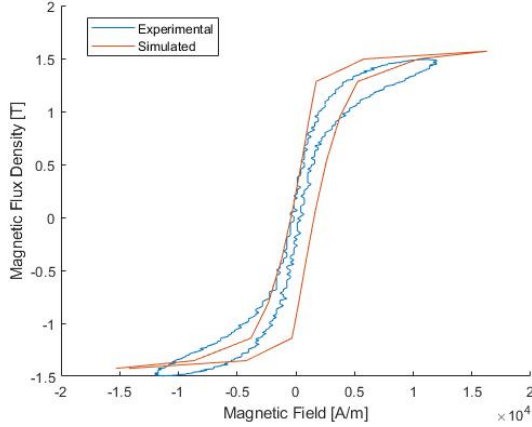


Figure 21: Experimental and simulated B(H) curve

Considering that the active power in the circuit iron + coil is given through equation (39)

$$P = U_{RMS} I_{RMS} \cos(\phi) \quad (39)$$

where ϕ is the phase angle between current and voltage. The phase angle can be compute using the equation (40)

$$\phi = \tan^{-1} \left(\frac{X_L}{R} \right) \quad (40)$$

where R is the DC resistance and X_L the reactance associated to the magnetic circuit.

In table 5 are represented the computed values for this simulation

Table 5: RMS voltage and current and power factor for simulated model iron + coil

U_{RMS} [V]	I_{RMS} [A]	$\cos(\phi)$
197.98	4.84	0.032

Considering (32), it is possible to compute the losses due to iron. Table 6 represent the total power and respective losses.

Table 6: Power and losses for simulated model iron + coil

P_T [W]	P_{Cu} [W]	P_{iron} [W]
30.65	19.89	10.76

It was developed another simulation with the design of figure 20. However, the simulation revels inconclusive results and due to that, it was impossible to compute the losses in YBCO through simulation.

6. Conclusions

6.1. Achievements

This dissertation is divided in two parts, the first one is related with the application of similitude laws through an analytic model for HTS. The second part is an attempt of experimental and simulated validation of this analytic model.

Regarding to the application of similitude laws, it was implemented the KIM model and was made an analytic study with emphasis on losses due to hysteresis in HTS. After that, and based on a background in similitude laws, it was possible to develop some scale relations for YBCO material. This relations allows a comparison between the conventional PM machines and machines where the YBCO can replace the PM or the copper coils. The major conclusion was that the modular configuration isn't the ideal solution when YBCO are considered.

In terms of experimental validation, three different experiments were developed, where only one, iron core solution, had results. However, this results were very different from the analytic model which leads to a simulated through FEM software to increase the precision.

6.2. Future Work

To guarantee a more broad spectrum of results, other types of electrical machines need to consider. Considering another type of electrical machine implies changing some relations of the scale laws, especially in considering if the current densities or the magnetic flux density remain constant, or if they have a dependency between one another.

Regarding the experimental part, the simulations need to be made in a more controllable environment, with more precision in the measurements, coupled with a consistent FEM model of the experimentations, to validate the results of the KIM model, and consequently, the scale laws.

References

- [1] J. Arnaud. *Use of superconductors in the excitation system of electric generators adapted to renewable energy sources*. Master's thesis, Instituto Superior Tecnico, Universidade de Lisboa, 2015.
- [2] D.-X.Chen and R.B.Goldfarb. *Kim model for magnetization of type-II superconductors*. Journal of Applied Physics 66, 2489, 1989.
- [3] J. Fernandes. *Gerador Eólico Polifásico de Fluxo Transverso com Magnetos Permanentes*. Master's thesis, Instituto Superior Tecnico, Universidade de Lisboa, 2011.
- [4] J. F. Gieras. *Superconducting Electrical Machines State of the Art*. Przegląd Elektrotechniczny, 2009.

- [5] P. Lobato. *Paradigmas Construtivos da Máquina Elétrica de Relutância Comutada*. PhD thesis, Faculdade de Ciências e Tecnologia, Universidade Nova de Lisboa, 2015.
- [6] S. S. Mircea Popescu and D. Zarko. *Scaling Laws for Synchronous Permanent Magnet Machines*. Tenth International Conference on Ecological Vehicles and Renewable Energies (EVER), 2015.
- [7] N. Pop and O. Caltun. *ALGORITHM TO DESCRIBE MAGNETIZATION CURVES BY USING JILES ATHERTON MODEL*. “Al. I. Cuza” University, Faculty of Physics Carpath Center, 700506 Iasi, Romania, 2010.
- [8] N. Pop and O. Caltun. *Jiles–Atherton Magnetic Hysteresis Parameters Identification*. “Al. I. Cuza” University, Faculty of Physics Carpath Center, 700506 Iasi, Romania, 2011.
- [9] A. L. Rodrigues. *New Electric Reluctance Motor with Bulk Superconducting Materials on the Rotor*. Kusadasi, 2001.
- [10] F. Silva. *ZFC Superconductor Magnetic Levitation System “Maglev-Tuga”*. Master’s thesis, Instituto Superior Técnico, Universidade de Lisboa, 2018.